

Response to the Referee

We are thankful to reviewers for their constructive comments and suggestions.

Reviewer: I find the paper acceptable if you indicate in your abstract that then DEMETER emissions are "non-free space", while the "terrestrial kilometric radiation" is free space. Maybe We show in this study the similarities and the discrepancies between the non-free space DEMETER frequency banded emissions and the well-known free space terrestrial kilometric radiation.

A: In the Abstract of the paper, we have corrected the corresponding sentence as suggested by the referee.

Low altitude frequency banded equatorial emissions observed below the electron cyclotron frequency

Mohammed Boudjada¹, Patrick Galopeau², Sami Sawas³, Valery Denisenko^{4,5}, Konrad Schwingenschuh¹, Helmut Lammer¹, Hans Eichelberger¹, Werner Magnes¹, and Bruno Besser¹

¹Space Research Institute, Austrian Academy of Sciences, Graz, Austria

²LATMOS-CNRS, Université Versailles Saint-Quentin-en-Yvelines, Guyancourt, France

³Institute of Communications and Wave Propagation, University of Technology, Graz, Austria

⁴Institute of Computational Modelling, Russian Academy of Sciences, Krasnoyarsk, Russia

⁵Siberian Federal University, Krasnoyarsk, Russia

Correspondence: M.Y. Boudjada (mohammed.boudjada@oeaw.ac.at)

Abstract. The ICE experiment onboard the DEMETER satellite recorded frequency banded wave emissions below the electron cyclotron frequency, with band spacing \gtrsim frequency low hybrid resonance, in the vicinity of the magnetic equatorial plane. Those radiations were observed in the beginning of the year 2010 on the night-side of the Earth and rarely on the day-side. We distinguish two components one appears as frequency bands continuous in time between few kHz and up to 50 kHz and the 5 other one from 50 kHz to 800 kHz. The first component exhibits positive and negative frequency drift rates in the southern and northern hemispheres, at latitudes between 40° and 20° . The second one displays multiple spaced frequency bands. Such bands mainly occur near the magnetic equatorial plane with a particular enhancement of the power level when the satellite latitude is close to the magnetic equatorial plane. [We show in this study the similarities and the discrepancies between DEMETER frequency banded emission and the well-known terrestrial kilometric radiation.](#) We show in this study the similarities and the 10 discrepancies between the non-free space DEMETER frequency banded emissions and the well-known free space terrestrial kilometric radiation. The hollow cones of the DEMETER frequency banded wave emissions are oriented towards the Earth's ionosphere. We suggest that the source region is localized in regions poleward of the plasmapause where the plasma frequency to gyro-frequency ratio is bigger than one.

Copyright statement. TEXT

15 1 Introduction

A variety of radio waves have been detected in the near Earth's space environment in the seventies. First type of waves were observed at frequencies below 100 kHz and up to 30 kHz (Brown, 1973), and even lower between 5 kHz and 20 kHz (Gurnett and Shaw, 1973). These two types of emission belong to a single non-thermal continuum spectrum, one 'trapped' and the other 'escaping' (Gurnett, 1975). Also high resolution spectrograms made evident the presence of numerous narrow-band

emissions for the 'escaping' component (Kurth et al., 1981). Later on, CLUSTER tetrahedral configuration of four identical satellites allowed the analysis of specific type of nonthermal continuum (Décréau et al., 2001). Direction finding technique, based on antenna spin modulation, allowed localizing the source regions in the plasmapause (Décréau et al., 2004) confirming previous GEOTAIL observations (Hashimoto et al., 1999). Grimald et al. (2008) showed in the nonthermal emissions the presence of spectral peaks organized as several banded emissions with a frequency interval nearby the gyrofrequency at the sources. The considered event was recorded on Dec., 30th, 2003, in the southern and northern hemispheres before and after plasmapause boundaries. All satellites display a similar behavior with arranged peaking times (i.e. C1, C2, and C3 then C4) corresponding to the satellite ordering along the line of pearls configuration. Authors suggested a stable beam of limited cone angle. Further polarization investigations of such type of banded emissions by Grimald and Santolik (2010) leaded to conclude that the observed polarization excludes the presence of Langmuir mode and the ordinary mode. Also details on the wave spectral signature was investigated by El-Lemdani Mazouz et al. (2009) particularly the splitting in fine frequency bands. Another type called 'nonthermal continuum patches' were found to occur within a relatively short time and over a wide frequency range (Grimald et al., 2011). Authors showed that plasmaspheric 'patches' events represent 25% of the total nonthermal emissions recorded in one year.

Also space observations provided by IMAGE satellite (Burch, 2000) allowed a better investigation of the inner plasmasphere. Radio Plasma Imager (RPI) was designed to use radio sounding technique leading the reception of echoes from remote plasma regions. Emitted pulses can propagate in the Z mode, and also the whistler mode (Carpenter et al., 2003). Hence signals detected at frequencies below the local upper hybrid frequency $f_{uh} = (f_p^2 + f_g^2)^{1/2}$ could propagate in the whistler and Z modes. Here f_p and f_g are the plasma frequency and the gyro-frequency, respectively. Sonwalkar et al. (2004) showed that the f_p/f_g ratio leads the sounding of different regions of the plasmasphere. Hence the condition $f_p/f_g > 1$ allows sounding below 2000 km and above 4000 km within the Earth's plasmasphere. In regions poleward of the plasmapause prevails the second condition, i.e. $f_p/f_g < 1$. Similar plasma conditions where derived from theoretical approach by Goertz and Strangeway (1995) using the Appleton-Hartree dispersion relation.

In this paper, we analyze the frequency banded radiation observed by ICE/DEMETER experiment in the beginning of the year 2010. The characteristics of this radiation, essentially the spectral features and the spatial occurrence are described in Section 2. Discussion of the outcomes is detailed in Section 3 where principally our results are combined to previous ones. Summary of the main results are given in Section 4.

2 Frequency banded wave emission

2.1 Overview of HF/ICE observations

We consider in this study the space observations provided by the DEMETER microsatellite. The aim is the analysis of particular spectral features recorded by the ICE experiment in the beginning of the year 2010, i.e. January, February and March. The ICE instrument allows a continuous survey of the electric field over a wide frequency range, from few Hz up to about 3.5 MHz (Berthelier et al., 2006). The electric field component is determined along the axis defined by two sensors. The satellite sun-

synchronous half-orbit duration is about 40 min and covering invariant latitude between -65° and $+65^\circ$. The DEMETER satellite orbits are associated to two fixed local times (LTs), at about 10 LT and 22 LT. We use in this investigation the survey mode of the ICE experiment covering the frequency range between few kHz and 3.5 MHz, called hereafter HF-band. The radio wave emissions are alternately recorded on the day- and night-sides of the Earth corresponding respectively to down and up half-orbits. However the main radiations investigated in this paper are observed on the night-side, and rarely on the day-side. Generally the ICE HF-band dynamic spectra allow distinguishing three kinds of spectral emissions depending on the satellite geographical latitudes. The first one is recorded close to the sub-auroral regions at latitudes between 50° and 60° ; it mainly concerns the auroral kilometric radiation described by Parrot and Berthelier (2012). The second are mainly ground-based transmitters, low frequency (LF) radiation, appearing at mid-latitudes between 50° and 20° , in both hemispheres (e.g., Parrot et al., 2009; Boudjada et al., 2017).

The third kind of emission is a frequency banded wave radiation occurring in the vicinity of the equatorial magnetic plane at low latitudes. Hereafter we focus on the analysis of the banded radiation in particular the spectral characteristics, the magnetic latitude and the power intensity occurrence. Also the dependence of the power level on the frequency and the magnetic latitude is considered. We use a manually technique which consists to follow and to save with the PC-computer mouse the frequency and the temporal evolution of the radiation. The saved parameters are the observation time (UT hours), the frequency (kHz) and the power level ($\mu V m^{-1} Hz^{-1/2}$). The collected points are later combined with the satellite orbital parameters like the magnetic latitude and the L-Shell.

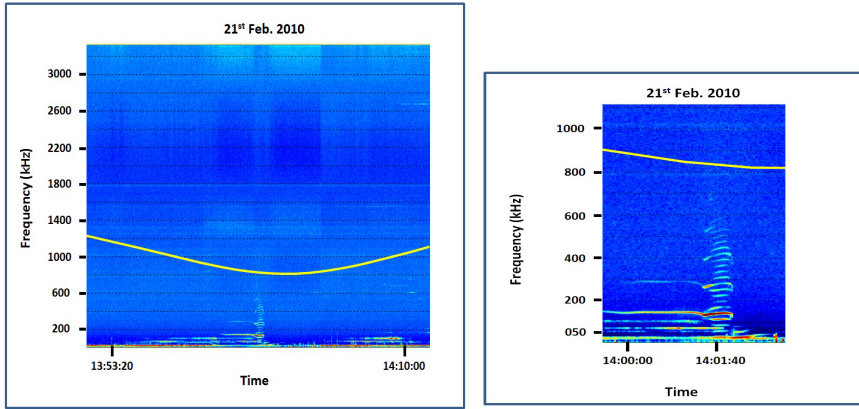


Figure 1. Example of frequency banded wave emission recorded by the ICE/DEMETER on 21st Feb. 2010. The first panel displays an overview of the dynamic spectrum in the frequency range from few kHz to 3.5 MHz. The second panel shows a zoomed part for the event in the frequency bandwidth between few kHz and 1100 kHz. The gyro-frequency is indicated by the yellow curve.

2.2 Frequency and time characteristics

The DEMETER ICE experiment detected frequency banded emissions in the frequency range between few kilohertz and up to 800 kHz. Two examples recorded on the night-side are shown in Fig.1 and Fig.2. First panel of Fig.1 displays the dynamic spectrum recorded by ICE experiment on 21st Feb. 2010 between 13:52 UT and 14:12 UT. The satellite was on the late evening 5 sector, around 22 LT, at a distance of 665 km. In this time interval the satellite geographical coordinate varied from -18°S to +04°N in latitude and 142° to 138° in longitude. The second event shown in the first panel of Fig.2 was also recorded at about 22 LT at similar distance from the Earth. Satellite geographical coordinate varied from -25°S to 40°N in latitude and 117° to 102° in longitude in the time interval between 14:10 UT and 14:26 UT. Second panel of Fig.1/Fig.2 displays a zoomed 10 part of the dynamic spectrum shown in the first panel where the emission appears in the frequency range between few kHz and up to 800 kHz. One note on both second panels of Fig.1 and Fig.2, changes in the spectral emissions before and after 50 kHz. Hence the first radiation appears as a narrow continuum with an instantaneous bandwidth of about 2 kHz at frequencies 15 less than 50 kHz. It displays negative and positive frequency drifts when the satellite is approaching or leaving the equatorial plane, respectively. Its frequency drift rate is weak and in the order of 0.2 kHz/s. The second emission is composed of parallel narrow-bands in a frequency above 50 kHz and up to 800 kHz. The band time duration is, on average, of about 1 minute and decreases to less than one minute when the emission frequency increases.

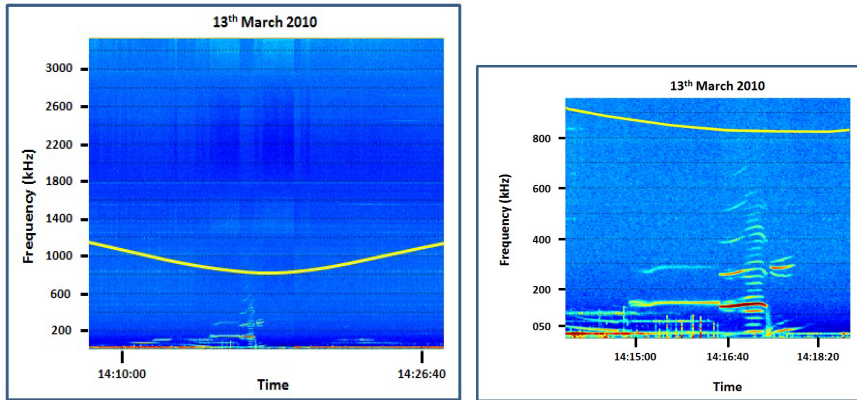


Figure 2. Like in Fig.1 for an event recorded by DEMETER on 13th March 2010.

The number of parallel narrow-bands are found to be different from one event to another. Hence we find, respectively, 18 and 20 parallel bands on 21st Feb. 2010 (Fig.1) and 13th March 2010 (Fig.2). The spacing of the frequency band, on average, is about 30 kHz when we consider both events. One can note that some narrow-bands showed a high power level (red color in Fig.1/Fig.2), when they are compared to other narrow bands, and also exhibit an extensive time duration of about few minutes. 20 Such enhanced narrow bands appear at 140 kHz, 270 kHz and 540 kHz in Fig.1, and at 130 kHz, 250 kHz, 410 kHz and 550 kHz. The enhanced banded frequencies above 200 kHz, may be considered as harmonic components of a 'fundamental'

frequency which appears around 140 kHz and which exhibits a longer time duration. It comes that five short weak narrow band emissions separate the basic frequency, i.e. 140 kHz, from its first harmonic around 280 kHz. Hereafter, we consider a statistical analysis of all events observed in January, February and March 2010.

2.3 Magnetic latitude and power level occurrence

5 The frequency banded radiation occurrences in magnetic latitude and power level are shown, respectively, in the top and the bottom panels of Fig.3. The main emission were recorded when DEMETER was in the southern part of the magnetic equatorial plane. Hence the emissions are detected in the magnetic latitude range between -40° and 20° , as shown in the first panel of Fig.3. We note a clear progressive increase of the frequency banded emission occurrence which reaches a maximum at magnetic latitude of -10° . More than 90% of the radiation occurred in magnetic latitude range between -30° and 0° . Sudden decrease of
10 the occurrence is recorded when the satellite crosses the magnetic equatorial plane. Emission is found to be more extended in the southern hemisphere with a clear di-symmetry occurrence before and after the equatorial magnetic plane.

The power level, as displayed in the second panel of Fig.3, is covering a large interval between $10^{-3} \mu Vm^{-1} Hz^{-1/2}$ and $10^{+4} \mu Vm^{-1} Hz^{-1/2}$. More than 70% of emissions have a level less than $1 \mu Vm^{-1} Hz^{-1/2}$ and belong mainly to the southern hemisphere. Above this weak power level, the occurrence of the frequency banded emission is associated to both hemispheres.

15 The intense power level is associated to the emission occurring mainly at lower frequency, i.e. from few kilohertz and up to 100 kHz. We distinguish three occurrence maxima at about $5 \times 10^{-3} \mu Vm^{-1} Hz^{-1/2}$, $1 \mu Vm^{-1} Hz^{-1/2}$ and $80 \mu Vm^{-1} Hz^{-1/2}$. We separate the power level by taking into consideration the interval associated to the previous maxima. Hereafter green, blue and red colors indicate, respectively, three power level intervals, i.e. $0.001 - 0.7 \mu Vm^{-1} Hz^{-1/2}$, $0.7 - 10 \mu Vm^{-1} Hz^{-1/2}$, and $10 - \mu Vm^{-1} Hz^{-1/2}$.
20 Frequency banded wave emissions are regularly observed on the night-side (22 LT) before and after the magnetic equatorial plane in the vicinity of the Earth at a distance less than 750 km. Fig.4 displays the daily occurrence of frequency banded emissions on 25th Feb. 2010. We observe a periodic occurrence of the emission with a time interval of about 1h35 which corresponds to a DEMETER microsatellite full orbit. Each vertical line is considered as an 'event' and corresponds to the recorded emission for a given half-orbit. The occurrence per day is about 13 events in the optimal case. However from one
25 event to another we find a variation in the frequency bandwidth and also in the power level.

2.4 Power level versus frequency and magnetic latitude

Fig.5 displays the power level variation versus the magnetic latitude where the colors indicate different power levels as defined in the previous sub-Section. The weakest intensities (less than $0.7 \mu Vm^{-1} Hz^{-1/2}$) are recorded at magnetic latitudes between -50° and $+30^\circ$ but much more in the southern hemisphere, as displayed in first panel of Fig.5. Structured emissions appear

30 when the magnetic latitude is positive principally after the crossing of the magnetic equatorial plane. One can distinguish five components appearing in four frequency ranges: few kHz - 50 kHz, 70 kHz - 130 kHz, 170 kHz - 250 kHz, 280 kHz - 340 kHz and 380 kHz- 420 kHz. Those radiations are extended in magnetic latitudes in particular at low frequencies around 50 kHz, and

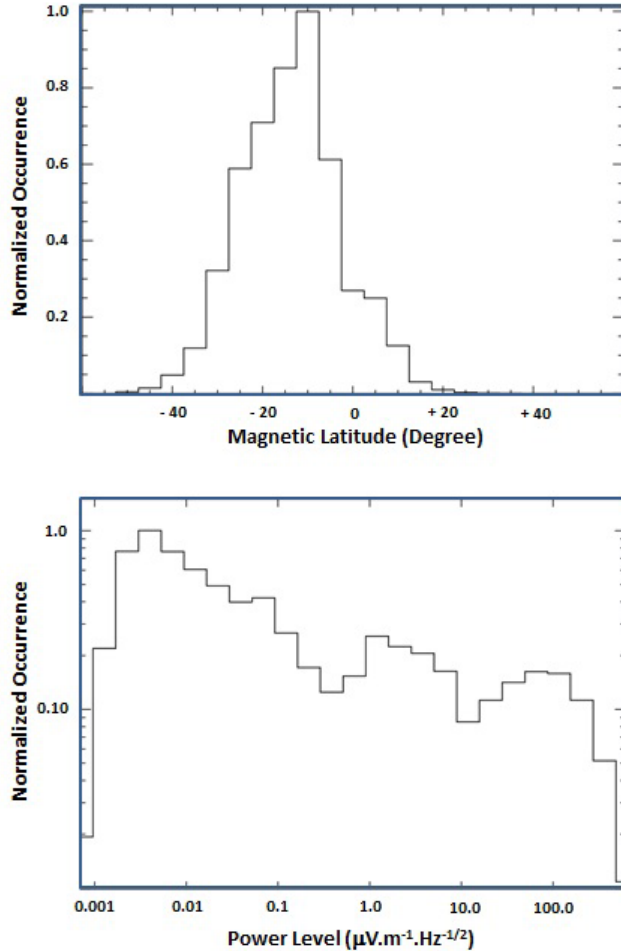


Figure 3. Occurrence of frequency banded radiations in magnetic latitude (Degree) and in power level ($\mu V m^{-1} Hz^{-1/2}$).

decreases at higher frequencies, at about 400 kHz. Frequency banded emission is quasi-absent between those four frequency bands.

Also structured emissions are observed in the southern part of the magnetic equatorial plane at frequencies above 200 kHz in magnetic latitude between -10° and 0° degrees, as shown in the first panel of Fig.5. Those structures are mainly extended 5 in frequency, contrary to those observed in northern hemisphere which extended in magnetic latitude. We distinguish four components occurring in the following frequency bands: 200 kHz - 320 kHz, 320 kHz - 450 kHz, 450 kHz - 570 kHz and 570 kHz - 670 kHz. At frequencies lower than 200 kHz, we note a quasi-absent of structured emission in the southern hemisphere. Radiations continuously occur in magnetic latitude between -50° and 0° . In this interval, we find a positive/negative frequency drift rate of about $+3.75 / -1.25$ kHz/degree when the frequency is higher/smaller than 50 kHz. The emissions is mainly

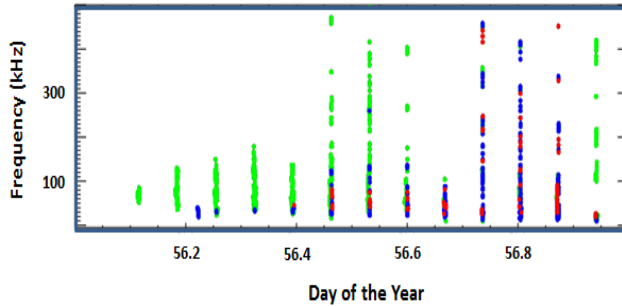


Figure 4. Vertical lines indicate the occurrence of the frequency banded emissions observed on 25th Feb. 2010. Those events were recorded on the night-side of the Earth with a time interval of about 01h35mnin. Green, blue and red colors specify, respectively, three power level intervals, i.e. $10^{-3} - 0.7 \mu Vm^{-1} Hz^{-1/2}$, $0.7 - 10 \mu Vm^{-1} Hz^{-1/2}$, and $10 - 10^{+4} \mu Vm^{-1} Hz^{-1/2}$.

confined to frequencies lower than 150/100 kHz in the southern/northern part of the magnetic equatorial plane when the power level is between 0.7 and $10 \mu Vm^{-1} Hz^{-1/2}$, as displayed in the second panel of Fig.5. Above 150 kHz, the radiations only occur in the frequency bandwidth 180 kHz to about 250 kHz. The power level in the range $10 - 10^4 \mu Vm^{-1} Hz^{-1/2}$ is shown in the third panel of Fig.5. The main emission is nearly symmetrical distributed around the magnetic equatorial plane, between -10° and $+10^\circ$, predominantly above 100 kHz. Below this limit, the radiation covers larger magnitude latitude from -20° to about $+20^\circ$.

The overlapping of the three power levels, as shown in Fig.6, allow getting a global shape similar to a 'tree' spectral pattern. We see globally that the frequency banded emission is extensively occurring at frequency lower than 150 kHz, and starts to be less confined to the magnetic equatorial plane above this frequency limit. A cut-off appears around 50 kHz which decrease to about few kHz when approaching the magnetic equator plane. This cut-off is characterized by a small frequency drift rate in latitude and a power level in the interval 0.7 and $10 \mu Vm^{-1} Hz^{-1/2}$, i.e. blue color boundary in Fig.6. A second cut-off can be seen when the DEMETER satellite was in the southern hemisphere and absent in northern hemisphere. It starts at latitudes of about -40° and disappears at -18° when the frequency decreases from 150 kHz to 50 kHz. We find that both cut-offs intersected at frequency of about 50 kHz when the magnitude latitude is about -18° .

Table 1 lists the main observational parameters derived from Fig.6. For each hemisphere is indicated the opening angle of the beam, the frequency range and the magnetic latitude. Schematic representations of those beams are given, respectively, in Fig.7 and Fig.8 for the southern and northern hemispheres.

3 Discussion

We discuss hereafter the frequency banded emission as detected by the DEMETER microsatellite. First we emphasize on the beaming of such emissions and how it extended and restrained around the magnetic equatorial plane. Then the similarity and

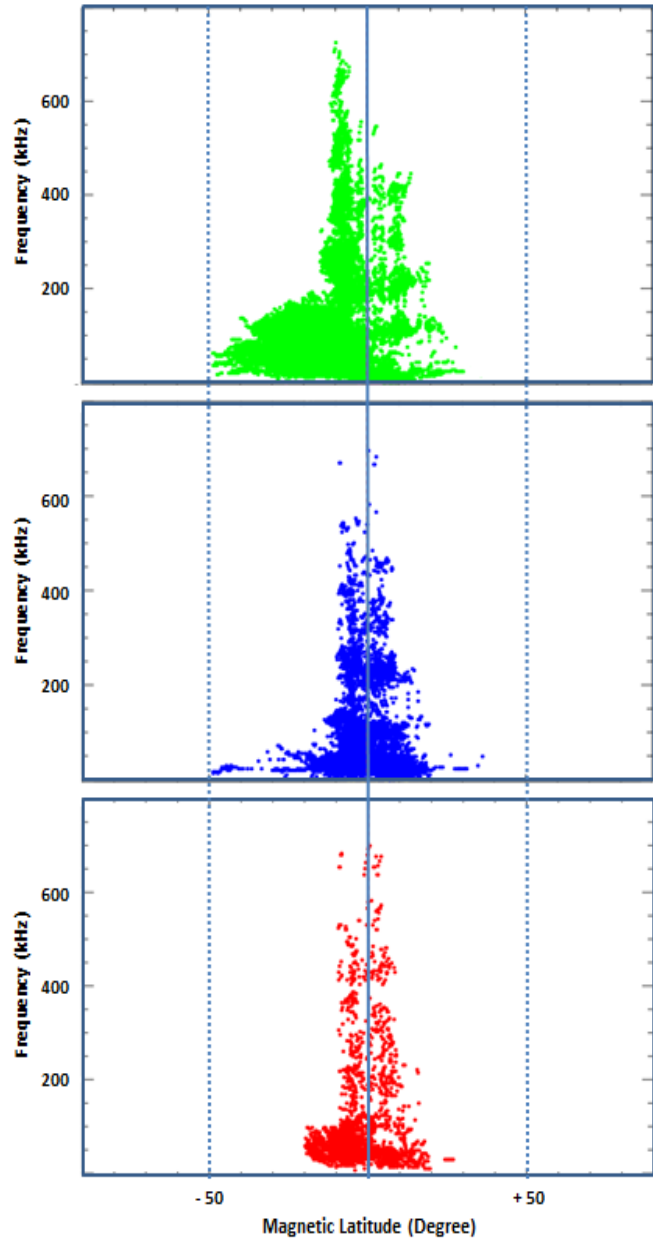


Figure 5. Variation of the power levels versus the frequency (vertical axis) and the magnetic latitude (horizontal axis) for all events. Colors are similar to those used in Fig.4. Green, blue and red colors specify, respectively, three power level intervals, i.e. $10^{-3} - 0.7 \mu Vm^{-1} Hz^{-1/2}$, $0.7 - 10 \mu Vm^{-1} Hz^{-1/2}$, and $10 - 10^{+4} \mu Vm^{-1} Hz^{-1/2}$.

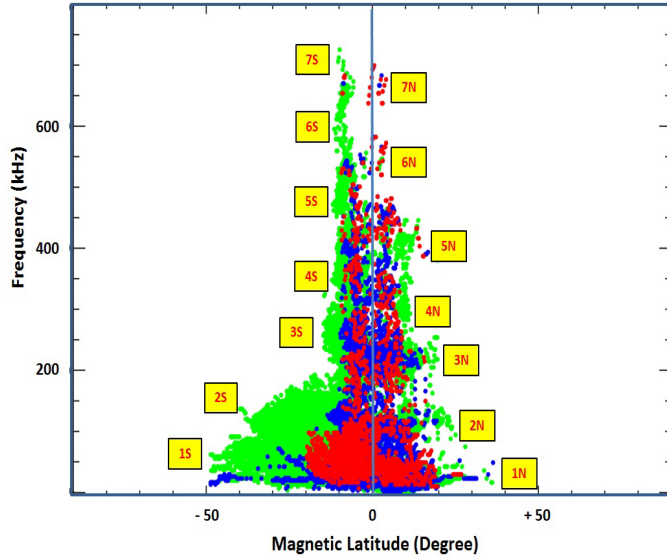


Figure 6. Overlapping of the three power levels displayed in Fig.5. The spectral pattern looks like a 'Christmas tree' with a 'trunk' along the magnetic equatorial plane. We have indicated by numbers the main parts of the spectral pattern for the southern and northern hemispheres. Table 1 lists the observational parameters associated to the investigated events.

the discrepancy between DEMETER frequency banded emission and the terrestrial kilometric radiations are addressed. This is followed by a discussion on the generation mode and the source location.

3.1 Beaming of the frequency banded emission

The passage of DEMETER satellite through the magnetic equator lead to characterize a frequency banded radiation recorded

- 5 in the vicinity of the magnetic equatorial plane. The capability of DEMETER satellite leads to regularly recorded such type of emission at low altitudes around 700 km. We have found that the radiations exhibit different spectral patterns when the frequency is smaller or bigger than 50 kHz. The satellite recorded emissions on both side of the magnetic equator, and they appear to be more structured bands in the northern hemisphere. Those lasting bands indicate a 'stable' features in the late evening sector at about 22 LT.
- 10 The power level distribution of the frequency banded emission shows restrained and extended deployment around the equatorial magnetic plane. Hence the latitudinal beam is found to be of about 40° when the frequency is, on average, less than 100 kHz. Above this limit and up to about 800 kHz, the latitudinal beam is decreasing and found of about 20°. This general picture is easily seen in the third panel of Fig.5. However we note a clear difference in the beam when the level is less than $1 \mu V m^{-1} Hz^{-1/2}$, as showed in the first panel of Fig.5. Hence the frequency banded wave radiation beam is different when
- 15 combining the emission recorded in the southern and northern parts of the magnetic equatorial plane. In the southern one, half of

Table 1. Observational parameters of the main parts of the spectral patterns as indicated in Fig.6.

Hemisphere	Point	Opening Angle	Frequency Range	Magnetic Latitude
Southern	1S	35°	30kHz ÷ 100kHz	-50° ÷ 0°
	2S	25°	100kHz ÷ 200kHz	-40° ÷ 0°
	3S	08°	200kHz ÷ 300kHz	-15° ÷ 0°
	4S	06°	300kHz ÷ 450kHz	-12° ÷ 0°
	5S	4.5°	450kHz ÷ 550kHz	-12° ÷ -5°
	6S	4°	550kHz ÷ 700kHz	-12° ÷ -6°
	7S	3.5°	700kHz ÷ 730kHz	-10° ÷ -6°
Northern	7N	2°	630kHz ÷ 700kHz	-2° ÷ 5°
	6N	2°	530kHz ÷ 580kHz	-3° ÷ 5°
	5N	7°	350kHz ÷ 480kHz	-2° ÷ 15°
	4N	7°	250kHz ÷ 350kHz	0° ÷ 12°
	3N	12°	150kHz ÷ 250kHz	0° ÷ 20°
	2N	18°	70kHz ÷ 150kHz	0° ÷ 25°
	1N	25°	30kHz ÷ 70kHz	0° ÷ 30°

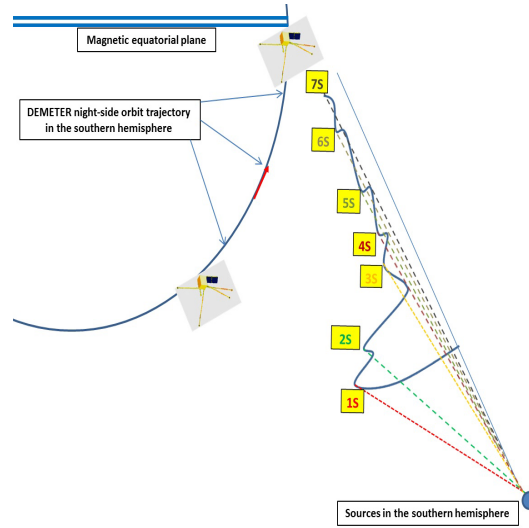


Figure 7. Sketch of the beams observed in the southern hemisphere for specific magnetic latitudes and frequencies (i.e. 1S, 2S, 3S, 4S, 5S, 6S and 7S) as listed in Table 1.

the spectral pattern is observed, i.e. beams of 25° and 10°, on average, in the frequency bandwidths 30 kHz-100 kHz and 100 kHz-800 kHz, respectively.

The beams of the frequency banded events are found to depend on the satellite orbits with regard to the magnetic equatorial plane as shown in Fig.7 and Fig.8. Beams associated to the southern hemisphere events are observed in different frequency bandwidth. We may be deal with two source regions localized in the southern part of the magnetic equator but confined to two unlike regions with high and low plasma densities. On the other side of the equatorial magnetic plane only branches, or limbs.

5 It is evident that emission diagrams are unlike which may be due to combine effects of multi-beams associated to sources localized in different regions. Beams in Fig.7 and Fig.8 may be considered as an overlapping of single beams. Each one can be associated to one narrow band structure as shown in Fig.1 and Fig.2.

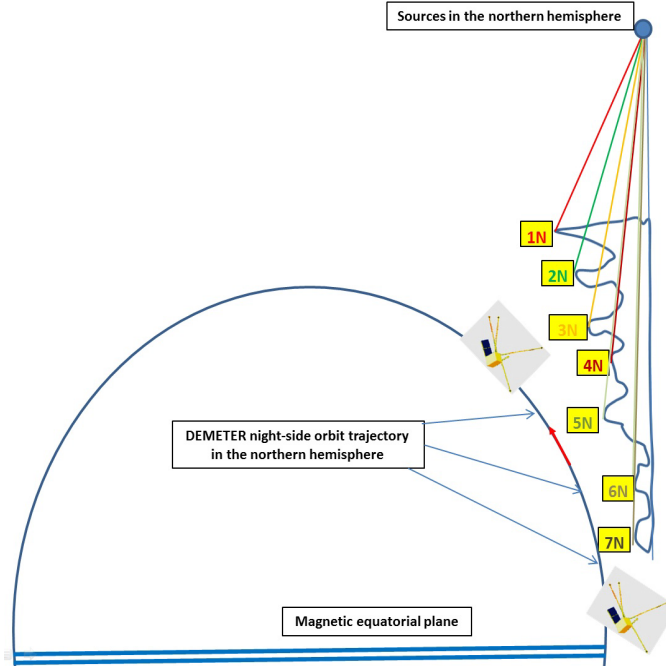


Figure 8. Sketch of the beams observed in the northern hemisphere for specific magnetic latitudes and frequencies (i.e. 1N, 2N, 3N, 4N, 5N, 6N and 7N) as listed in Table 1.

Fig.9 displays the variation of the L-shell associated to the frequency banded events versus magnetic latitude of the satellite. The power level is principally found to increase between 1 and 1.4 L-shell when the magnetic latitude of DEMETER is in 10 between -20° and $+20^\circ$. Those orbital parameters are related to the beam radiated by the source emission which crossed DEMETER trajectories.

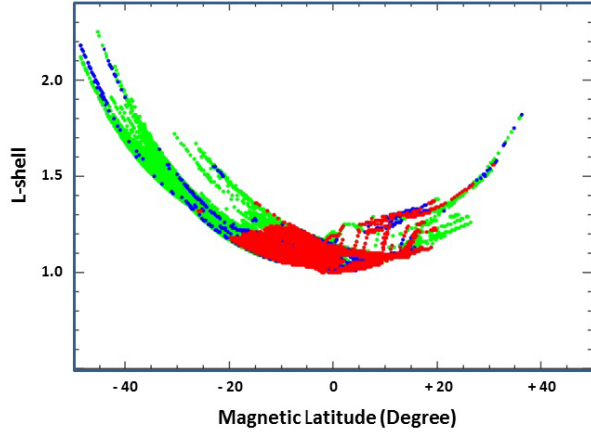


Figure 9. Variation of the frequency banded wave emission versus the L-Shell and the magnetic latitude.

3.2 Similarity and discrepancy with the terrestrial kilometric emission

Frequency banded emission features, as investigated in this paper, allow us to address questions concerning its origin. We have found some spectral patterns which are similar to those reported in the literature in the case of the terrestrial kilometric emissions.

5 First, we have described changes of the spectral emissions at frequencies of about 50 kHz. Such frequencies boundaries are similar to those observed by other satellite observations, like Cluster, GEOTAIL and IMAGE. Hence the terrestrial kilometric radiation is trapped and escaping when the frequency is, respectively, smaller and bigger than 50 kHz. The spectral features are often comparable and the main alternations may be due to the instrumental time and frequency resolutions, and also the satellite orbits with regard to the source locations. Hence Green and Boardsen (2006) show a typical sample of the kilometric

10 continuum recorded by RPI/IMAGE experiment during a passage of the magnetic equator plane. In their Fig.2, one can observe the presence of parallel narrow bands at frequencies above 30 kHz. Such narrow bands have morphological similarity with those displayed in Fig.6 of our paper. AKR-X/INTERBALL-1 experiment provided similar emissions particularly in the southern hemisphere at low magnetic latitude and at L-Shell of about 1.2 as reported by Kuril'chik et al. (2001, 2007). Observations at fixed frequencies (100 kHz, 252 kHz, 500 kHz and 749 kHz) allowed the analysis of the spectral character of such emissions.

15 Authors showed that the terrestrial kilometric radiation occurrence is depending on the solar activity. Such radiation is regularly recorded during quiet solar activity. Our observations were registered in the beginning of the year 2010, nearly eighteen months after the minimum of solar activity, i.e. Aug. 2008. Also the spectral pattern looks like a 'Christmas-tree' as also reported by Green and Boardsen (2006) in their review about the kilometric continuum radiation and it is confined to the magnetic equatorial plane.

20 Despite those common spectral features, several other observational aspects are different when combining the terrestrial kilometric radiation and the frequency banded wave emission. The investigated DEMETER emission is detected at distance

of about $1.1R_E$ which is generally not the case of the terrestrial kilometric emission. For instance GEOTAIL and CLUSTER observations recorded radiation at more than $15R_E$ as reported by Hashimoto et al. (1999) and (Décréau et al., 2004), respectively. Also, the trapped or the escaping component is linked to terrestrial kilometric radiation recorded, respectively, between the plasmasphere and the magnetosphere, or outside of the magnetosphere. This radiation propagate largely in the free space

5 in the L-O mode above the local plasma frequency linked to sources at or very near the plasmapause (Hashimoto et al., 2006). Also the gyro-frequency is found to be smaller than the trapped and the escaping frequencies as recorded by RPI/IMAGE experiment (see Fig.2 of Green and Boardsen (2006)). All those observational parameters are not similar to those reported in the case of the frequency banded wave emission recorded by DEMETER satellite.

3.3 Micro-scale features of the inner part of the plasmasphere

10 It is clear that both radiations have common spectral features but several discrepancy observational aspects linked to the generation mechanism. However the source locations should be the plasmasphere. Hence the terrestrial kilometric radiation is linked to plasmaspheric sources with emission beams oriented towards the magnetosphere. Fig.7 and 8 showed the emission beams which interact with DEMETER orbits. The sources are localized in polaward of the plasmasphere. This means that the DEMETER orbits is crossing the plasmaspheric hollow cones on few dozen of kilometer. Probably such restricted regions

15 may be associated to the Z-mode waves which are linked to the free escaping L-O mode as suggested by Jones (1976) in his model. In such region the Z-mode waves are considered to be trapped and later converted into L-O mode associated to the terrestrial kilometric radiation. Later on Goertz and Strangeway (1995) derived from the Appleton-Hartree dispersion relation the whistler wave propagation in the case when the electron plasma frequency is greater than the gyro-frequency. Carpenter et al. (2003) found similar region where ray paths of Z-mode echoes from radio sounding were recorded by IMAGE

20 satellite in the polar regions. Also Sonwalkar et al. (2004) investigated the whistler mode echoes from radio sounding and found f_p smaller than f_g in the region poleward of the plasmapause. Green and Boardsen (2006) investigated and reported about the linear mode conversion theory based on Jones model. Authors showed profiles of plasmaspheric plasma frequency taking into consideration the Z-mode and the equatorial gyro-frequency. Regions of sharp plasma gradient are found and shown in Fig.5 of their paper.

25 We estimate the relationship between the Z-mode frequency (f_z), the plasma frequency (f_p) and the gyro-frequency (f_g) using the following formulae: $f_z = (f_g/2)[-1 + (1 + 4(f_p/f_g)^2)^{1/2}]$ (Carpenter et al., 2003). Fig.10 displays the variation of the three frequencies (i.e. f_z , f_p and f_g) versus the geocentric distance. The trapping region is localized between the lower and the higher f_z (green color in Fig.10) mainly between 1 kHz and 100 kHz, and extended up to 700 kHz. The plasma frequency is following the trapping region and starting at about 10 kHz and up to 800 kHz. The gyro-frequency appears at

30 higher frequencies, i.e. above 800 kHz. Those features are comparable to previous investigations, e.g. Gurnett et al. (1983) and Carpenter et al. (2003) in polar regions.

It is important to note that the frequency banded emissions may be due to the interaction and/or the co-existence of electrostatic and whistler waves. Hence Bell and Ngo (1990) considered theoretically the generation, in the case of density cavity or gradient, of whistler waves by lower hybrid waves. Such co-existence of both waves have been investigated by An et al.

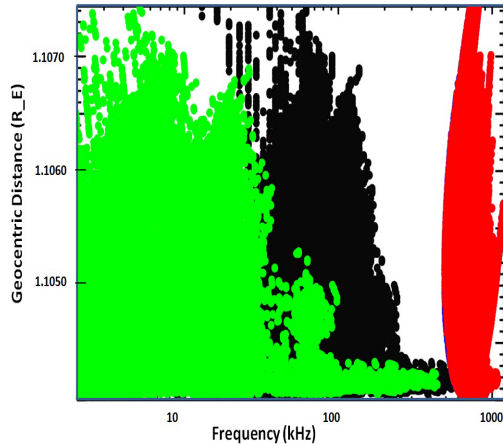


Figure 10. Variations of the frequency banded emission versus the geocentric distance expressed in R_E . The green, black and red colors are associated, respectively, to f_z , f_p and f_g frequencies.

(2017) using Darwin particle-in-cell (PIC) simulation. Such models have been recently invoked by Vartanyan et al. (2016) and Li et al. (2017) in the investigation, respectively, of generation of whistler waves and chorus wave modulation observed onboard DEMETER and Van Allen Probes satellites.

4 Conclusion

- 5 We have investigated the frequency banded wave radiation recorded by ICE/DEMETER experiment. DEMETER orbits allow us to regularly record this radiation where, in the optimal case, about 13 events are daily registered. The power level is found in the interval between $10^{-3} \mu Vm^{-1}Hz^{-1/2}$ and $10^{+4} \mu Vm^{-1}Hz^{-1/2}$. The spectral analysis leads to find a 'tree spectral shape' which is the traces of the beaming of the frequency banded wave radiation. We have shown that those beams are not similar and depend on the emission frequency and the magnetic latitude. DEMETER frequency banded emission can be
- 10 comparable to the well-known terrestrial kilometric radiation. However several other observational aspects are different when combining both emissions in particular the generation modes. We suggest that the DEMETER frequency banded emissions are linked to a Z-mode micro-scale region. This trapping Z-mode region can only be detected between the Earth's ionosphere and the plasmasphere. The hollow cones of this frequency banded wave emissions are crossed by the DEMETER orbits at altitudes lower than 700 km. Probably the source regions of the DEMETER frequency banded emission should be the plasmasphere,
- 15 like the terrestrial kilometric radiation. IMAGE investigations reported about density structures recorded by EUV experiment (Burch, 2000) where new terms have been defined like channels and crenulations (Darrouzet et al., 2009), and also a time evolution of the plasmasphere in particular on the pre-midnight sector (Sandel et al., 2003). We may consider that DEMETER

orbits allow to investigate the inner part of the plasmasphere when other missions (i.e. GEOTAIL, IMAGE, INTERBALL) lead to study the outer part of the plasmasphere.

Acknowledgements. Acknowledgements. We acknowledge C. N. E. S. for the use of the DEMETER data, and thankful to Jean-Jacques Berthelier who provided us with data from the electric field experiment (Instrument Champ Électrique – ICE).

References

An, X., Bortnik, J., Van Compernolle, B., Decyk, V., and R. Thorne, Electrostatic and whistler instabilities excited by an electron beam, *Physics of Plasmas*, 24, 072116, 2017.

Bell, T.F., and H.D. Ngo, Electrostatic lower hybrid waves excited by electromagnetic whistler mode waves scattering from planar magnetic-field-aligned plasma density irregularities, *J. Geophys. Res.*, 95, A1, 149–172, 1990.

Berthelier, J.J., Godefroy, M., Leblanc, F., Malingre, M., Menvielle, M., Lagoutte, D., Brochot, J.Y., Colin, F., Elie, F., Legendre, C., Zamora, P., Benoist, D., Chapuis, Y., Artru, J., and R. Pfaff, ICE, the electric field experiment on DEMETER, *Planet. Space Sci.*, 54, 456–471, 2006.

Boudjada, M.Y., P.F. Biagi, E. Al-Haddad, P.H.M. Galopeau, B. Besser, D. Wolbang, G. Prattes, H. Eichelberger, G. Stangl, M. Parrot and K. Schwingenschuh, Reception conditions of low frequency (LF) transmitter signals onboard DEMETER micro-satellite, *Physics and Chemistry of the Earth*, 102, 70–79, 2017.

Brown, L.W., The galactic radio spectrum between 130 kHz and 2600 kHz, *Astrophys. J.*, 359–370, 1973.

Burch, J.L., IMAGE mission overview, *Space Sci. Rev.*, 91, 1–14, 2000.

Carpenter, D.L., Bell, T.F., Inan, U.S., Benson, R.F., Sonwalkar, V.S., Reinisch, B.W., and D. L. Gallagher, Z-mode sounding within propagation "cavities" and other inner magnetospheric regions by the RPI instrument on the IMAGE satellite, *J. Geophys. Res.*, 108, A12, 2003.

Darrouzet, F., Gallagher, D. L., André, N., Carpenter, D. L., Dandouras, I., Décréau, P. M. E., De Keyser, J., Denton, R. E., Foster, J. C., Goldstein, J., Moldwin, M. B., Reinisch, B. W., Sandel, B. R., and J. Tu, Plasmaspheric Density Structures and Dynamics: Properties Observed by the CLUSTER and IMAGE Missions, *Space Sci. Rev.*, 145, 55–106, 2009.

Décréau, P. M. E., Ducoin, C., Le Rouzic, G., Randriamboarison, O., Rauch, J.-L., Trotignon, J.-G., Vallières, X., Canu, P., Darrouzet, F., Gough, M. P., Buckley, A. M., and T.D. Carozzi, Observation of continuum radiations from the Cluster fleet: first results from direction finding, *Ann. Geophys.*, 22, 2607-2624, 2004.

Décréau, P. M. E., Fergeau, P., Krasnoselskikh, V., Le Guirriec, E., Lévéque, M., Martin, Ph., Randriamboarison, O., Rauch, J. L., Senée, F. X., Séran, H. C., Trotignon, J. G., Canu, P., Cornilleau, N., de Féraudy, H., Alleyne, H., Yearby, K., Mögensen, P. B., Gustafsson, G., André, M., Gurnett, D. C., Darrouzet, F., Lemaire, J., Harvey, C. C., Travnicek, P., and Whisper experimenters: Early results from the Whisper instrument on Cluster: an overview, *Ann. Geophys.*, 19, 1241-1258, 2001.

El-Lemdani Mazouz, F., J. L. Rauch, P. M. E. Décréau, J. G. Trotignon, X. Vallières, F. Darrouzet, P. Canu, and X. Suraud, Wave emissions at half electron gyroharmonics in the equatorial plasmasphere region: CLUSTER observations and statistics, *Adv. Space Res.*, 43, 253-264, 2009.

Goertz, C. K., and R. J. Strangeway, Plasma waves, in *Introduction to Space Physics*, edited by M. G. Kivelson and C. T. Russell, p. 356, Cambridge Univ. Press, New York, 1995.

Green, J. L., and S. A. Boardsen, Kilometric continuum radiation, *Radio Sci. Bull.*, 318, 34- 41, 2006.

Green, J. L., S. Boardsen, S. F. Fung, H. Matsumoto, K. Hashimoto, R. R. Anderson, B. R. Sandel, and B. W. Reinisch, Association of kilometric continuum radiation with plasmaspheric structures, *J. Geophys. Res.*, 109, A03203, 2004.

Grimald, S., and O. Santolik, Possible wave modes of wideband nonthermal continuum radiation in its source region, *J. Geophys. Res.*, 115, A06209, 2010.

Grimald, S., El-Lemdani Mazouz, F., Foullon, C., Décréau, P. M. E., Boardsen, S. A., and X. Vallières, X.: Study of non-thermal continuum patches: wave propagation and plasmapause study, *J. Geophys. Res.*, 116, A07219, 2011.

Grimald, S., Décréau, P. M. E., Canu, P., Rochel, A., and X. Vallières, Medium latitude sources of plasmaspheric non thermal continuum radiations observed close to harmonics of the electron gyrofrequency, *J. Geophys. Res.*, 113, A11217, 2008.

5 Gurnett, D. A., The Earth as a radio source: The nonthermal continuum, *J. Geophys. Res.*, 80, 2751–2763, 1975.

Gurnett, D. A., and L. A. Frank, Continuum radiation associated with low-energy electrons in the outer radiation zone, *J. Geophys. Res.*, 81, 3875–3885, 1976.

Gurnett, D. A., and R. A. Shaw, Electromagnetic radiation trapped in the magnetosphere above the plasma frequency, *J. Geophys. Res.*, 78, 8136- 8148, 1973.

10 Gurnett, D. A., Shawhan, S.D., and R. R. Shaw, Auroral hiss, Z-mode radiation, and auroral kilometric radiation in the polar magnetosphere: DE 1 observations, *J. Geophys. Res.*, 88, 329, 1983.

Hashimoto, K., J. L. Green, R. R. Anderson, and H. Matsumoto, Review of kilometric continuum, in *Geospace Electromagnetic Waves and Radiation*, Lect. Not. in Phys., Eds. J. W. LaBelle and R. A. Treumann, Springer, New York, 687, 37–54, 2006.

Hashimoto, K., W. Calvert, and H. Matsumoto, Kilometric continuum detected by GEOTAIL, *J. Geophys. Res.*, 104, 28,645- 28,656, 1999.

15 Jones, D., Source of terrestrial nonthermal radiation, *Nature*, 260, 686-689, 1976.

Kuril'chik, V.N., M. Y. Boudjada, H. O. Rucker, and I. F. Kopaeva, Observations of Electromagnetic Emissions inside the Earth's Plasmasphere from the INTERBALL-1 Satellite, *Cosmic Res.*, 45, 455–460, 2007.

Kuril'chik, V.N., Boudjada, M.Y. and H.O. Rucker, INTERBALL-1 observations of the plasmaspheric emissions related to terrestrial 'continuum' radio emissions, in *Planetary Radio Emissions V*, Eds. Rucker, H.O., Kaiser, M.L., and Leblanc, Y., Vienna: Austrian Academy of Sciences Press, 325–335, 2001.

20 Kurth, W. S., D. A. Gurnett, and R. R. Anderson, Escaping nonthermal continuum radiation, *J. Geophys. Res.*, 86, 5519–5531, 1981.

Li, J., Bortnik, J., An, X., Li, W., Thorne, R.M., Zhou, M., Kurth, W.S., Hospodarsky, G.B., Funsten, H.O., and H.E. Spence, Chorus Wave Modulation of Langmuir Waves in the Radiation Belts, *Geophys. Res. Lett.*, 44, 11713–11721, 2017.

Parrot M. and J.-J. Berthelier, AKR-like emissions observed at low altitude by the DEMETER satellite, *J. Geophys. Res.*, 117, A10314,

25 2012.

Parrot, M., U. S. Inan, N. G. Lehtinen, and J. L. Pincon, Penetration of lightning MF signals to the upper ionosphere over VLF ground-based transmitters, *J. Geophys. Res.*, 114, A12318, 2009.

Sandel, B.R., J. Goldstein, D.L. Gallagher and M. Spasojevic, Extreme ultraviolet imager observations of the structure and dynamics of the plasmasphere. *Space Sci. Rev.*, 109, 25-46 2003.

30 Sonwalkar, V.S., D.L. Carpenter, T.F. Bell, M. Spasojevic, U.S. Inan, J. Li, X. Chen, A. Venkatasubramanian, J. Harikumar, R.F. Benson, W.W.L. Taylor, and B. W. Reinisch, Diagnostics of magnetospheric electron density and irregularities at altitudes <5000 km using whistler and Z mode echoes from radio sounding on the IMAGE satellite, *J. Geophys. Res.*, 109, A11212, 2004.

Vartanyan, A., Milikh, G.M., Eliasson, B., Najmi, A.C., Parrot, M., and K. Papadopoulos, Generation of whistler waves by continuous HF heating of the upper ionosphere, *Radio Sci.*, 51, 1188–1198, 2016.

Low altitude frequency banded equatorial emissions observed below the electron cyclotron frequency

Mohammed Boudjada¹, Patrick Galopeau², Sami Sawas³, Valery Denisenko^{4,5}, Konrad Schwingenschuh¹, Helmut Lammer¹, Hans Eichelberger¹, Werner Magnes¹, and Bruno Besser¹

¹Space Research Institute, Austrian Academy of Sciences, Graz, Austria

²LATMOS-CNRS, Université Versailles Saint-Quentin-en-Yvelines, Guyancourt, France

³Institute of Communications and Wave Propagation, University of Technology, Graz, Austria

⁴Institute of Computational Modelling, Russian Academy of Sciences, Krasnoyarsk, Russia

⁵Siberian Federal University, Krasnoyarsk, Russia

Correspondence: M.Y. Boudjada (mohammed.boudjada@oeaw.ac.at)

Abstract. The ICE experiment onboard the DEMETER satellite recorded frequency banded wave emissions below the electron cyclotron frequency, with band spacing \gtrsim frequency low hybrid resonance, in the vicinity of the magnetic equatorial plane. Those radiations were observed in the beginning of the year 2010 on the night-side of the Earth and rarely on the day-side. We distinguish two components one appears as frequency bands continuous in time between few kHz and up to 50 kHz and the other one from 50 kHz to 800 kHz. The first component exhibits positive and negative frequency drift rates in the southern and northern hemispheres, at latitudes between 40° and 20° . The second one displays multiple spaced frequency bands. Such bands mainly occur near the magnetic equatorial plane with a particular enhancement of the power level when the satellite latitude is close to the magnetic equatorial plane. We show in this study the similarities and the discrepancies between the non-free space DEMETER frequency banded emissions and the well-known free space terrestrial kilometric radiation. The hollow cones of the DEMETER frequency banded wave emissions are oriented towards the Earth's ionosphere. We suggest that the source region is localized in regions poleward of the plasmapause where the plasma frequency to gyro-frequency ratio is bigger than one.

Copyright statement. TEXT

1 Introduction

A variety of radio waves have been detected in the near Earth's space environment in the seventies. First type of waves were observed at frequencies below 100 kHz and up to 30 kHz (Brown, 1973), and even lower between 5 kHz and 20 kHz (Gurnett and Shaw, 1973). These two types of emission belong to a single non-thermal continuum spectrum, one 'trapped' and the other 'escaping' (Gurnett, 1975). Also high resolution spectrograms made evident the presence of numerous narrow-band emissions for the 'escaping' component (Kurth et al., 1981). Later on, CLUSTER tetrahedral configuration of four identical

satellites allowed the analysis of specific type of nonthermal continuum (Décréau et al., 2001). Direction finding technique, based on antenna spin modulation, allowed localizing the source regions in the plasmapause (Décréau et al., 2004) confirming previous GEOTAIL observations (Hashimoto et al., 1999). Grimald et al. (2008) showed in the nonthermal emissions the presence of spectral peaks organized as several banded emissions with a frequency interval nearby the gyrofrequency at the 5 sources. The considered event was recorded on Dec., 30th, 2003, in the southern and northern hemispheres before and after plasmapause boundaries. All satellites display a similar behavior with arranged peaking times (i.e. C1, C2, and C3 then C4) corresponding to the satellite ordering along the line of pearls configuration. Authors suggested a stable beam of limited cone angle. Further polarization investigations of such type of banded emissions by Grimald and Santolik (2010) leaded to conclude that the observed polarization excludes the presence of Langmuir mode and the ordinary mode. Also details on the wave spec-10 tral signature was investigated by El-Lemdani Mazouz et al. (2009) particularly the splitting in fine frequency bands. Another type called 'nonthermal continuum patches' were found to occur within a relatively short time and over a wide frequency range (Grimald et al., 2011). Authors showed that plasmaspheric 'patches' events represent 25% of the total nonthermal emissions recorded in one year.

Also space observations provided by IMAGE satellite (Burch, 2000) allowed a better investigation of the inner plasmas-15 sphere. Radio Plasma Imager (RPI) was designed to use radio sounding technique leading the reception of echoes from remote plasma regions. Emitted pulses can propagate in the Z mode, and also the whistler mode (Carpenter et al., 2003). Hence signals detected at frequencies below the local upper hybrid frequency $f_{uh} = (f_p^2 + f_g^2)^{1/2}$ could propagate in the whistler and Z modes. Here f_p and f_g are the plasma frequency and the gyro-frequency, respectively. Sonwalkar et al. (2004) showed that the f_p/f_g ratio leads the sounding of different regions of the plasmasphere. Hence the condition $f_p/f_g > 1$ allows sounding 20 below 2000 km and above 4000 km within the Earth's plasmasphere. In regions poleward of the plasmapause prevails the second condition, i.e. $f_p/f_g < 1$. Similar plasma conditions where derived from theoretical approach by Goertz and Strangeway (1995) using the Appleton-Hartree dispersion relation.

In this paper, we analyze the frequency banded radiation observed by ICE/DEMETER experiment in the beginning of the year 2010. The characteristics of this radiation, essentially the spectral features and the spatial occurrence are described in 25 Section 2. Discussion of the outcomes is detailed in Section 3 where principally our results are combined to previous ones. Summary of the main results are given in Section 4.

2 Frequency banded wave emission

2.1 Overview of HF/ICE observations

We consider in this study the space observations provided by the DEMETER microsatellite. The aim is the analysis of particular 30 spectral features recorded by the ICE experiment in the beginning of the year 2010, i.e. January, February and March. The ICE instrument allows a continuous survey of the electric field over a wide frequency range, from few Hz up to about 3.5 MHz (Berthelier et al., 2006). The electric field component is determined along the axis defined by two sensors. The satellite sun-synchronous half-orbit duration is about 40 min and covering invariant latitude between -65° and +65°. The DEMETER

satellite orbits are associated to two fixed local times (LTs), at about 10 LT and 22 LT. We use in this investigation the survey mode of the ICE experiment covering the frequency range between few kHz and 3.5 MHz, called hereafter HF-band. The radio wave emissions are alternately recorded on the day- and night-sides of the Earth corresponding respectively to down and up half-orbits. However the main radiations investigated in this paper are observed on the night-side, and rarely on the day-side. Generally the ICE HF-band dynamic spectra allow distinguishing three kinds of spectral emissions depending on the satellite geographical latitudes. The first one is recorded close to the sub-auroral regions at latitudes between 50° and 60° ; it mainly concerns the auroral kilometric radiation described by Parrot and Berthelier (2012). The second are mainly ground-based transmitters, low frequency (LF) radiation, appearing at mid-latitudes between 50° and 20° , in both hemispheres (e.g., Parrot et al., 2009; Boudjada et al., 2017).

The third kind of emission is a frequency banded wave radiation occurring in the vicinity of the equatorial magnetic plane at low latitudes. Hereafter we focus on the analysis of the banded radiation in particular the spectral characteristics, the magnetic latitude and the power intensity occurrence. Also the dependence of the power level on the frequency and the magnetic latitude is considered. We use a manually technique which consists to follow and to save with the PC-computer mouse the frequency and the temporal evolution of the radiation. The saved parameters are the observation time (UT hours), the frequency (kHz) and the power level ($\mu V m^{-1} Hz^{-1/2}$). The collected points are later combined with the satellite orbital parameters like the magnetic latitude and the L-Shell.

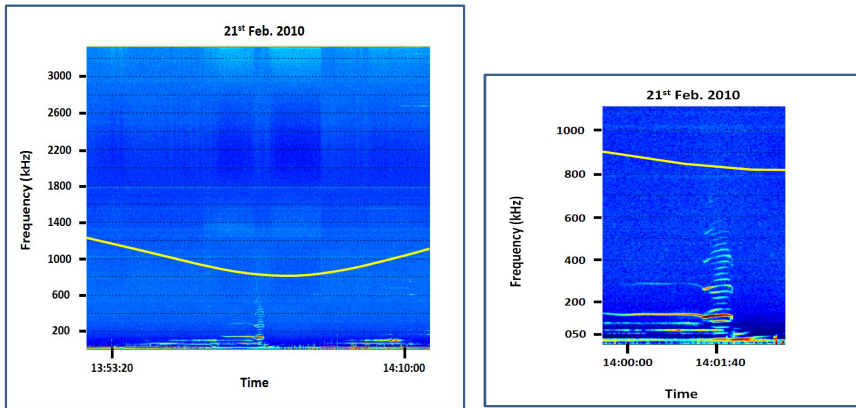


Figure 1. Example of frequency banded wave emission recorded by the ICE/DEMETER on 21st Feb. 2010. The first panel displays an overview of the dynamic spectrum in the frequency range from few kHz to 3.5 MHz. The second panel shows a zoomed part for the event in the frequency bandwidth between few kHz and 1100 kHz. The gyro-frequency is indicated by the yellow curve.

2.2 Frequency and time characteristics

The DEMETER ICE experiment detected frequency banded emissions in the frequency range between few kilohertz and up to 800 kHz. Two examples recorded on the night-side are shown in Fig.1 and Fig.2. First panel of Fig.1 displays the dynamic

spectrum recorded by ICE experiment on 21st Feb. 2010 between 13:52 UT and 14:12 UT. The satellite was on the late evening sector, around 22 LT, at a distance of 665 km. In this time interval the satellite geographical coordinate varied from -18°S to +04°N in latitude and 142° to 138° in longitude. The second event shown in the first panel of Fig.2 was also recorded at about 22 LT at similar distance from the Earth. Satellite geographical coordinate varied from -25°S to 40°N in latitude and 117° to 102° in longitude in the time interval between 14:10 UT and 14:26 UT. Second panel of Fig.1/Fig.2 displays a zoomed part of the dynamic spectrum shown in the first panel where the emission appears in the frequency range between few kHz and up to 800 kHz. One note on both second panels of Fig.1 and Fig.2, changes in the spectral emissions before and after 50 kHz. Hence the first radiation appears as a narrow continuum with an instantaneous bandwidth of about 2 kHz at frequencies less than 50 kHz. It displays negative and positive frequency drifts when the satellite is approaching or leaving the equatorial plane, respectively. Its frequency drift rate is weak and in the order of 0.2 kHz/s. The second emission is composed of parallel narrow-bands in a frequency above 50 kHz and up to 800 kHz. The band time duration is, on average, of about 1 minute and decreases to less than one minute when the emission frequency increases.

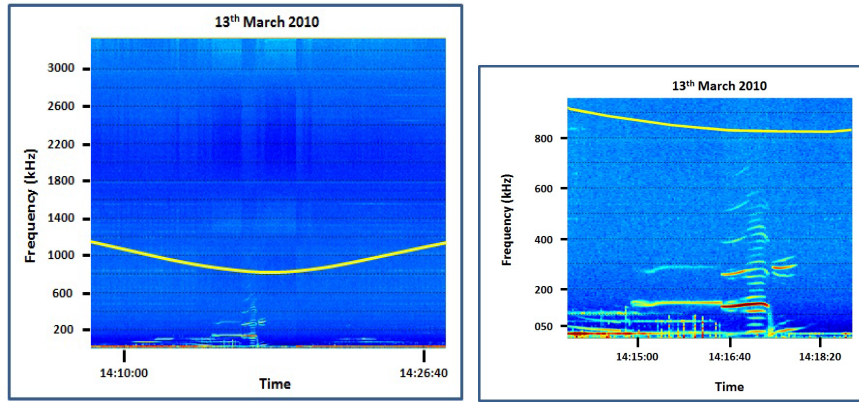


Figure 2. Like in Fig.1 for an event recorded by DEMETER on 13th March 2010.

The number of parallel narrow-bands are found to be different from one event to another. Hence we find, respectively, 18 and 20 parallel bands on 21st Feb. 2010 (Fig.1) and 13th March 2010 (Fig.2). The spacing of the frequency band, on average, 15 is about 30 kHz when we consider both events. One can note that some narrow-bands showed a high power level (red color in Fig.1/Fig.2), when they are compared to other narrow bands, and also exhibit an extensive time duration of about few minutes. Such enhanced narrow bands appear at 140 kHz, 270 kHz and 540 kHz in Fig.1, and at 130 kHz, 250 kHz, 410 kHz and 20 550 kHz. The enhanced banded frequencies above 200 kHz, may be considered as harmonic components of a 'fundamental' frequency which appears around 140 kHz and which exhibits a longer time duration. It comes that five short weak narrow band emissions separate the basic frequency, i.e. 140 kHz, from its first harmonic around 280 kHz. Hereafter, we consider a statistical analysis of all events observed in January, February and March 2010.

2.3 Magnetic latitude and power level occurrence

The frequency banded radiation occurrences in magnetic latitude and power level are shown, respectively, in the top and the bottom panels of Fig.3. The main emission were recorded when DEMETER was in the southern part of the magnetic equatorial plane. Hence the emissions are detected in the magnetic latitude range between -40° and 20° , as shown in the first panel of Fig.3. We note a clear progressive increase of the frequency banded emission occurrence which reaches a maximum at magnetic latitude of -10° . More than 90% of the radiation occurred in magnetic latitude range between -30° and 0° . Sudden decrease of the occurrence is recorded when the satellite crosses the magnetic equatorial plane. Emission is found to be more extended in the southern hemisphere with a clear di-symmetry occurrence before and after the equatorial magnetic plane.

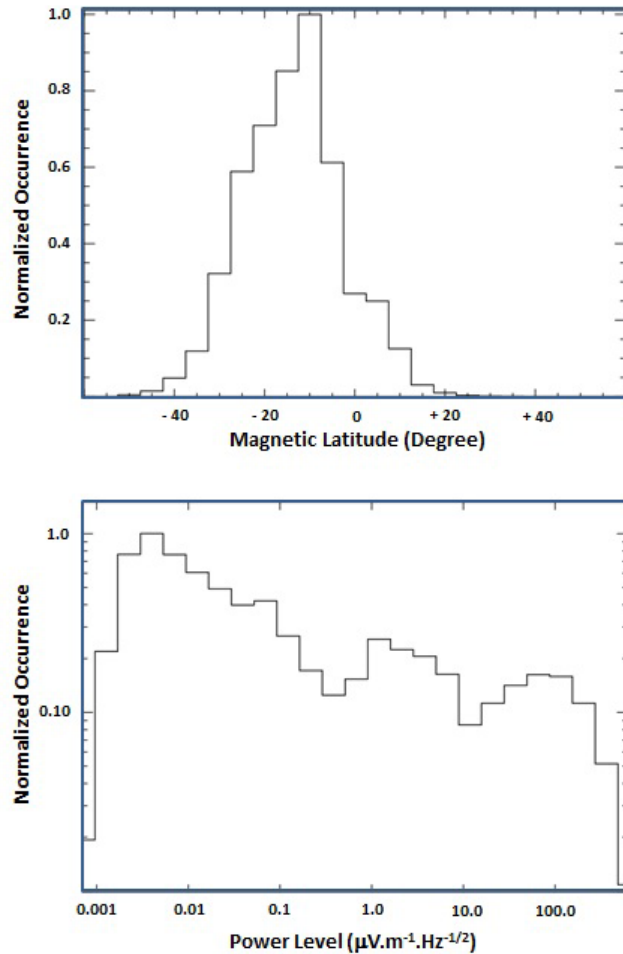


Figure 3. Occurrence of frequency banded radiations in magnetic latitude (Degree) and in power level ($\mu V m^{-1} Hz^{-1/2}$).

The power level, as displayed in the second panel of Fig.3, is covering a large interval between $10^{-3} \mu Vm^{-1}Hz^{-1/2}$ and $10^{+4} \mu Vm^{-1}Hz^{-1/2}$. More than 70% of emissions have a level less than $1 \mu Vm^{-1}Hz^{-1/2}$ and belong mainly to the southern hemisphere. Above this weak power level, the occurrence of the frequency banded emission is associated to both hemispheres. The intense power level is associated to the emission occurring mainly at lower frequency, i.e. from few kilohertz and up to 100 kHz. We distinguish three occurrence maxima at about $5 \times 10^{-3} \mu Vm^{-1}Hz^{-1/2}$, $1 \mu Vm^{-1}Hz^{-1/2}$ and $80 \mu Vm^{-1}Hz^{-1/2}$. We separate the power level by taking into consideration the interval associated to the previous maxima. Hereafter green, blue and red colors indicate, respectively, three power level intervals, i.e. $0.001 - 0.7 \mu Vm^{-1}Hz^{-1/2}$, $0.7 - 10 \mu Vm^{-1}Hz^{-1/2}$, and $10 - 10^{+4} \mu Vm^{-1}Hz^{-1/2}$.

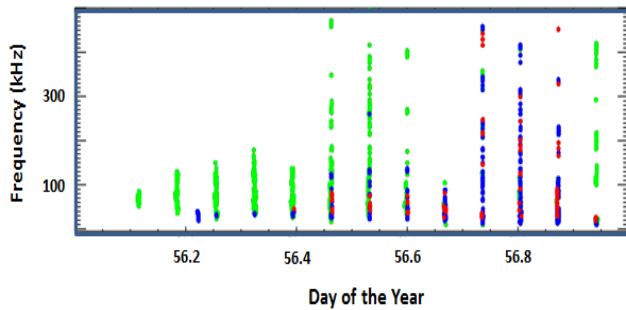


Figure 4. Vertical lines indicate the occurrence of the frequency banded emissions observed on 25th Feb. 2010. Those events were recorded on the night-side of the Earth with a time interval of about 01h35mnin. Green, blue and red colors specify, respectively, three power level intervals, i.e. $10^{-3} - 0.7 \mu Vm^{-1}Hz^{-1/2}$, $0.7 - 10 \mu Vm^{-1}Hz^{-1/2}$, and $10 - 10^{+4} \mu Vm^{-1}Hz^{-1/2}$.

Frequency banded wave emissions are regularly observed on the night-side (22 LT) before and after the magnetic equatorial plane in the vicinity of the Earth at a distance less than 750 km. Fig.4 displays the daily occurrence of frequency banded emissions on 25th Feb. 2010. We observe a periodic occurrence of the emission with a time interval of about 1h35 which corresponds to a DEMETER microsatellite full orbit. Each vertical line is considered as an 'event' and corresponds to the recorded emission for a given half-orbit. The occurrence per day is about 13 events in the optimal case. However from one event to another we find a variation in the frequency bandwidth and also in the power level.

15 2.4 Power level versus frequency and magnetic latitude

Fig.5 displays the power level variation versus the magnetic latitude where the colors indicate different power levels as defined in the previous sub-Section. The weakest intensities (less than $0.7 \mu Vm^{-1}Hz^{-1/2}$) are recorded at magnetic latitudes between -50° and $+30^\circ$ but much more in the southern hemisphere, as displayed in first panel of Fig.5. Structured emissions appear when the magnetic latitude is positive principally after the crossing of the magnetic equatorial plane. One can distinguish five components appearing in four frequency ranges: few kHz - 50 kHz, 70 kHz - 130 kHz, 170 kHz - 250 kHz, 280 kHz -340 kHz and 380 kHz- 420 kHz. Those radiations are extended in magnetic latitudes in particular at low frequencies around 50 kHz, and

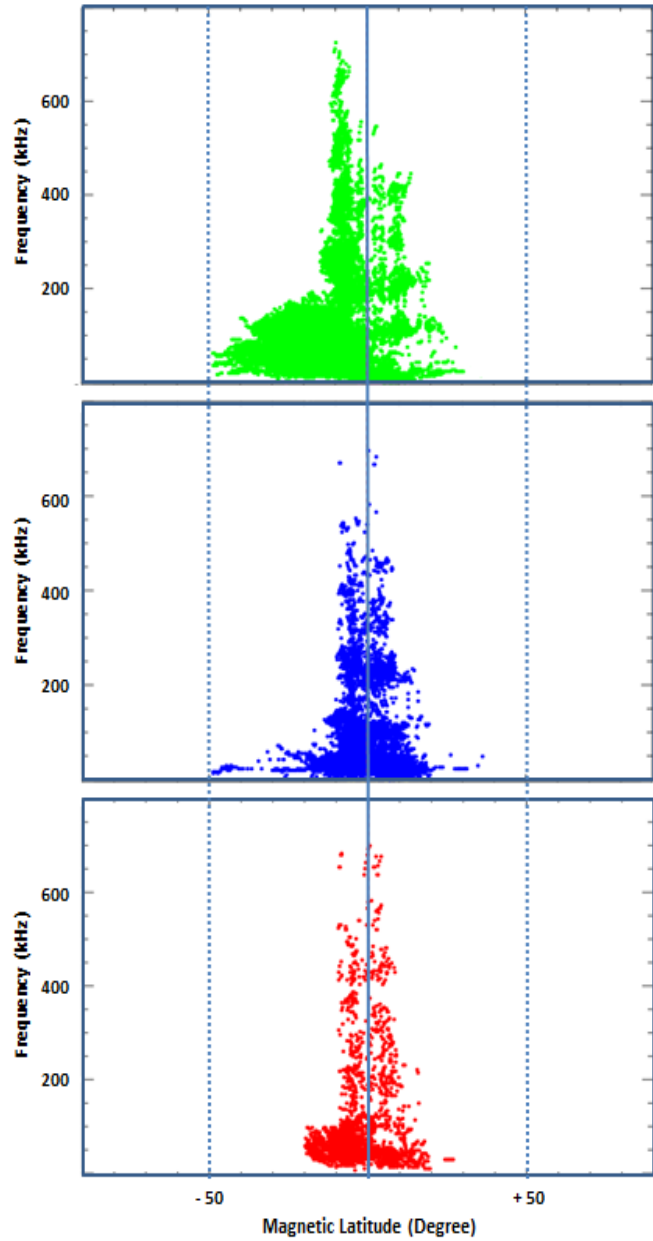


Figure 5. Variation of the power levels versus the frequency (vertical axis) and the magnetic latitude (horizontal axis) for all events. Colors are similar to those used in Fig.4. Green, blue and red colors specify, respectively, three power level intervals, i.e. $10^{-3} - 0.7 \mu Vm^{-1} Hz^{-1/2}$, $0.7 - 10 \mu Vm^{-1} Hz^{-1/2}$, and $10 - 10^{+4} \mu Vm^{-1} Hz^{-1/2}$.

decreases at higher frequencies, at about 400 kHz. Frequency banded emission is quasi-absent between those four frequency bands.

Also structured emissions are observed in the southern part of the magnetic equatorial plane at frequencies above 200 kHz in magnetic latitude between -10° and 0° degrees, as shown in the first panel of Fig.5. Those structures are mainly extended 5 in frequency, contrary to those observed in northern hemisphere which extended in magnetic latitude. We distinguish four components occurring in the following frequency bands: 200 kHz - 320 kHz, 320 kHz - 450 kHz, 450 kHz - 570 kHz and 570 kHz - 670 kHz. At frequencies lower than 200 kHz, we note a quasi-absent of structured emission in the southern hemisphere. Radiations continuously occur in magnetic latitude between -50° and 0° . In this interval, we find a positive/negative frequency 10 drift rate of about $+3.75 / -1.25$ kHz/degree when the frequency is higher/smaller than 50 kHz. The emissions is mainly confined to frequencies lower than 150/100 kHz in the southern/northern part of the magnetic equatorial plane when the power level is between 0.7 and $10 \mu V m^{-1} Hz^{-1/2}$, as displayed in the second panel of Fig.5. Above 150 kHz, the radiations only occur in the frequency bandwidth 180 kHz to about 250 kHz. The power level in the range $10 - 10^4 \mu V m^{-1} Hz^{-1/2}$ is shown in the third panel of Fig.5. The main emission is nearly symmetrical distributed around the magnetic equatorial plane, between -10° and $+10^\circ$, predominantly above 100 kHz. Below this limit, the radiation covers larger magnitude latitude from -20° to about $+20^\circ$.

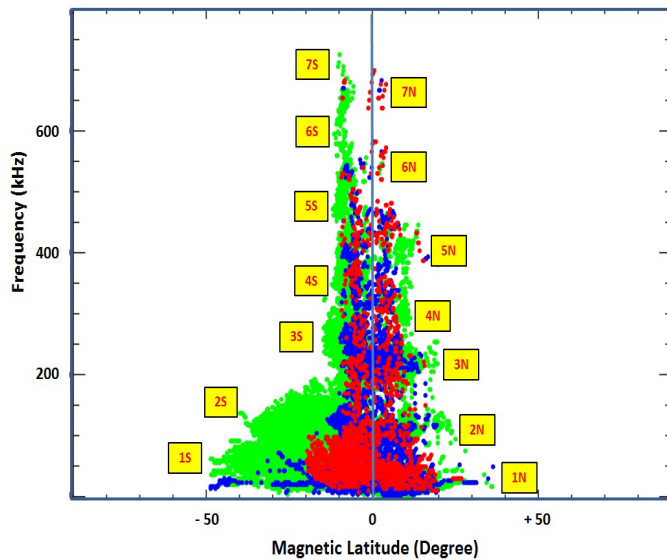


Figure 6. Overlapping of the three power levels displayed in Fig.5. The spectral pattern looks like a 'Christmas tree' with a 'trunk' along the magnetic equatorial plane. We have indicated by numbers the main parts of the spectral pattern for the southern and northern hemispheres. Table 1 lists the observational parameters associated to the investigated events.

15

The overlapping of the three power levels, as shown in Fig.6, allow getting a global shape similar to a 'tree' spectral pattern. We see globally that the frequency banded emission is extensively occurring at frequency lower than 150 kHz, and starts to be

Table 1. Observational parameters of the main parts of the spectral patterns as indicated in Fig.6.

Hemisphere	Point	Opening Angle	Frequency Range	Magnetic Latitude
Southern	1S	35°	30kHz ÷ 100kHz	-50° ÷ 0°
	2S	25°	100kHz ÷ 200kHz	-40° ÷ 0°
	3S	08°	200kHz ÷ 300kHz	-15° ÷ 0°
	4S	06°	300kHz ÷ 450kHz	-12° ÷ 0°
	5S	4.5°	450kHz ÷ 550kHz	-12° ÷ -5°
	6S	4°	550kHz ÷ 700kHz	-12° ÷ -6°
	7S	3.5°	700kHz ÷ 730kHz	-10° ÷ -6°
Northern	7N	2°	630kHz ÷ 700kHz	-2° ÷ 5°
	6N	2°	530kHz ÷ 580kHz	-3° ÷ 5°
	5N	7°	350kHz ÷ 480kHz	-2° ÷ 15°
	4N	7°	250kHz ÷ 350kHz	0° ÷ 12°
	3N	12°	150kHz ÷ 250kHz	0° ÷ 20°
	2N	18°	70kHz ÷ 150kHz	0° ÷ 25°
	1N	25°	30kHz ÷ 70kHz	0° ÷ 30°

less confined to the magnetic equatorial plane above this frequency limit. A cut-off appears around 50 kHz which decrease to about few kHz when approaching the magnetic equator plane. This cut-off is characterized by a small frequency drift rate in latitude and a power level in the interval 0.7 and $10 \mu V m^{-1} Hz^{-1/2}$, i.e. blue color boundary in Fig.6. A second cut-off can be seen when the DEMETER satellite was in the southern hemisphere and absent in northern hemisphere. It starts at latitudes of 5 about -40° and disappears at -18° when the frequency decreases from 150 kHz to 50 kHz. We find that both cut-offs intersected at frequency of about 50 kHz when the magnitude latitude is about -18°.

Table 1 lists the main observational parameters derived from Fig.6. For each hemisphere is indicated the opening angle of the beam, the frequency range and the magnetic latitude. Schematic representations of those beams are given, respectively, in Fig.7 and Fig.8 for the southern and northern hemispheres.

10 3 Discussion

We discuss hereafter the frequency banded emission as detected by the DEMETER microsatellite. First we emphasize on the beaming of such emissions and how it extended and restrained around the magnetic equatorial plane. Then the similarity and the discrepancy between DEMETER frequency banded emission and the terrestrial kilometric radiations are addressed. This is followed by a discussion on the generation mode and the source location.

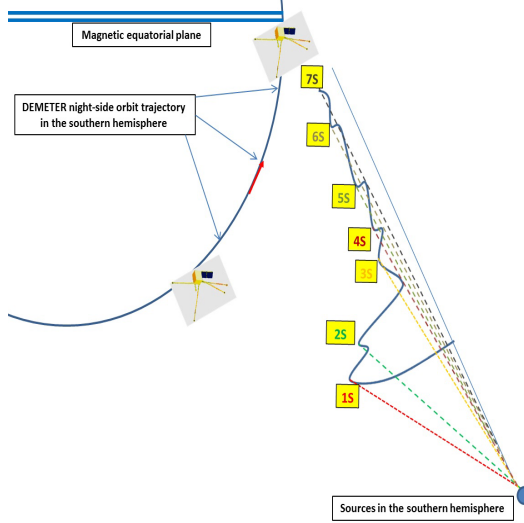


Figure 7. Sketch of the beams observed in the southern hemisphere for specific magnetic latitudes and frequencies (i.e. 1S, 2S, 3S, 4S, 5S, 6S and 7S) as listed in Table 1.

3.1 Beaming of the frequency banded emission

The passage of DEMETER satellite through the magnetic equator lead to characterize a frequency banded radiation recorded in the vicinity of the magnetic equatorial plane. The capability of DEMETER satellite leads to regularly recorded such type of emission at low altitudes around 700 km. We have found that the radiations exhibit different spectral patterns when the frequency is smaller or bigger than 50 kHz. The satellite recorded emissions on both side of the magnetic equator, and they appear to be more structured bands in the northern hemisphere. Those lasting bands indicate a 'stable' features in the late evening sector at about 22 LT.

The power level distribution of the frequency banded emission shows restrained and extended deployment around the equatorial magnetic plane. Hence the latitudinal beam is found to be of about 40° when the frequency is, on average, less than 100 kHz. Above this limit and up to about 800 kHz, the latitudinal beam is decreasing and found of about 20° . This general picture is easily seen in the third panel of Fig.5. However we note a clear difference in the beam when the level is less than $1 \mu V m^{-1} Hz^{-1/2}$, as showed in the first panel of Fig.5. Hence the frequency banded wave radiation beam is different when combining the emission recorded in the southern and northern parts of the magnetic equatorial plane. In the southern one, half of the spectral pattern is observed, i.e. beams of 25° and 10° , on average, in the frequency bandwidths 30 kHz-100 kHz and 100 kHz-800 kHz, respectively.

The beams of the frequency banded events are found to depend on the satellite orbits with regard to the magnetic equatorial plane as shown in Fig.7 and Fig.8. Beams associated to the southern hemisphere events are observed in different frequency bandwidth. We may be deal with two source regions localized in the southern part of the magnetic equator but confined to two

unlike regions with high and low plasma densities. On the other side of the equatorial magnetic plane only branches, or limbs. It is evident that emission diagrams are unlike which may be due to combine effects of multi-beams associated to sources localized in different regions. Beams in Fig.7 and Fig.8 may be considered as an overlapping of single beams. Each one can be associated to one narrow band structure as shown in Fig.1 and Fig.2.

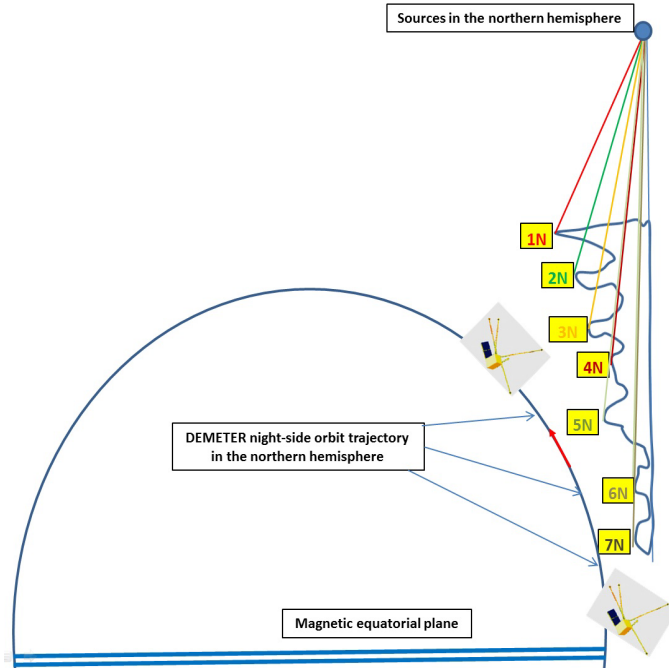


Figure 8. Sketch of the beams observed in the northern hemisphere for specific magnetic latitudes and frequencies (i.e. 1N, 2N, 3N, 4N, 5N, 6N and 7N) as listed in Table 1.

5 Fig.9 displays the variation of the L-shell associated to the frequency banded events versus magnetic latitude of the satellite. The power level is principally found to increase between 1 and 1.4 L-shell when the magnetic latitude of DEMETER is in between -20° and $+20^\circ$. Those orbital parameters are related to the beam radiated by the source emission which crossed DEMETER trajectories.

3.2 Similarity and discrepancy with the terrestrial kilometric emission

10 Frequency banded emission features, as investigated in this paper, allow us to address questions concerning its origin. We have found some spectral patterns which are similar to those reported in the literature in the case of the terrestrial kilometric emissions.

First, we have described changes of the spectral emissions at frequencies of about 50 kHz. Such frequencies boundaries are similar to those observed by other satellite observations, like Cluster, GEOTAIL and IMAGE. Hence the terrestrial kilometric

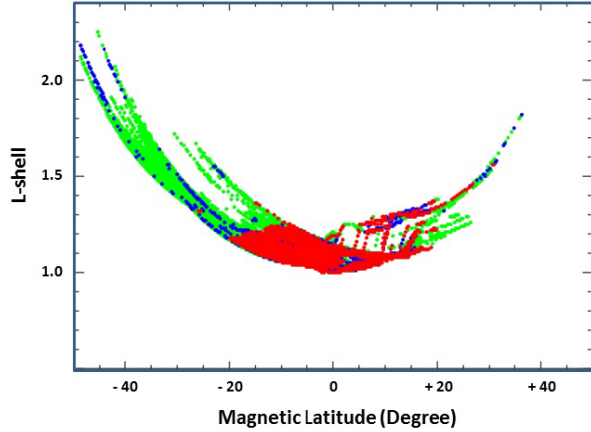


Figure 9. Variation of the frequency banded wave emission versus the L-Shell and the magnetic latitude.

radiation is trapped and escaping when the frequency is, respectively, smaller and bigger than 50 kHz. The spectral features are often comparable and the main alternations may be due to the instrumental time and frequency resolutions, and also the satellite orbits with regard to the source locations. Hence Green and Boardsen (2006) show a typical sample of the kilometric continuum recorded by RPI/IMAGE experiment during a passage of the magnetic equator plane. In their Fig.2, one can observe

5 the presence of parallel narrow bands at frequencies above 30 kHz. Such narrow bands have morphological similarity with those displayed in Fig.6 of our paper. AKR-X/INTERBALL-1 experiment provided similar emissions particularly in the southern hemisphere at low magnetic latitude and at L-Shell of about 1.2 as reported by Kuril'chik et al. (2001, 2007). Observations at fixed frequencies (100 kHz, 252 kHz, 500 kHz and 749 kHz) allowed the analysis of the spectral character of such emissions. Authors showed that the terrestrial kilometric radiation occurrence is depending on the solar activity. Such radiation is regularly
10 recorded during quiet solar activity. Our observations were registered in the beginning of the year 2010, nearly eighteen months after the minimum of solar activity, i.e. Aug. 2008. Also the spectral pattern looks like a 'Christmas-tree' as also reported by Green and Boardsen (2006) in their review about the kilometric continuum radiation and it is confined to the magnetic equatorial plane.

Despite those common spectral features, several other observational aspects are different when combining the terrestrial
15 kilometric radiation and the frequency banded wave emission. The investigated DEMETER emission is detected at distance of about $1.1R_E$ which is generally not the case of the terrestrial kilometric emission. For instance GEOTAIL and CLUSTER observations recorded radiation at more than $15R_E$ as reported by Hashimoto et al. (1999) and (Décréau et al., 2004), respectively. Also, the trapped or the escaping component is linked to terrestrial kilometric radiation recorded, respectively, between the plasmasphere and the magnetosphere, or outside of the magnetosphere. This radiation propagates largely in the free space
20 in the L-O mode above the local plasma frequency linked to sources at or very near the plasmapause (Hashimoto et al., 2006). Also the gyro-frequency is found to be smaller than the trapped and the escaping frequencies as recorded by RPI/IMAGE

experiment (see Fig.2 of Green and Boardsen (2006)). All those observational parameters are not similar to those reported in the case of the frequency banded wave emission recorded by DEMETER satellite.

3.3 Micro-scale features of the inner part of the plasmasphere

It is clear that both radiations have common spectral features but several discrepancy observational aspects linked to the 5 generation mechanism. However the source locations should be the plasmasphere. Hence the terrestrial kilometric radiation is linked to plasmaspheric sources with emission beams oriented towards the magnetosphere. Fig.7 and 8 showed the emission beams which interact with DEMETER orbits. The sources are localized in polaward of the plasmasphere. This means that the DEMETER orbits is crossing the plasmaspheric hollow cones on few dozen of kilometer. Probably such restricted regions 10 may be associated to the Z-mode waves which are linked to the free escaping L-O mode as suggested by Jones (1976) in his model. In such region the Z-mode waves are considered to be trapped and later converted into L-O mode associated to the terrestrial kilometric radiation. Later on Goertz and Strangeway (1995) derived from the Appleton-Hartree dispersion relation the whistler wave propagation in the case when the electron plasma frequency is greater than the gyro-frequency. Carpenter et al. (2003) found similar region where ray paths of Z-mode echoes from radio sounding were recorded by IMAGE 15 satellite in the polar regions. Also Sonwalkar et al. (2004) investigated the whistler mode echoes from radio sounding and found f_p smaller than f_g in the region poleward of the plasmapause. Green and Boardsen (2006) investigated and reported about the linear mode conversion theory based on Jones model. Authors showed profiles of plasmaspheric plasma frequency taking into consideration the Z-mode and the equatorial gyro-frequency. Regions of sharp plasma gradient are found and shown in Fig.5 of their paper.

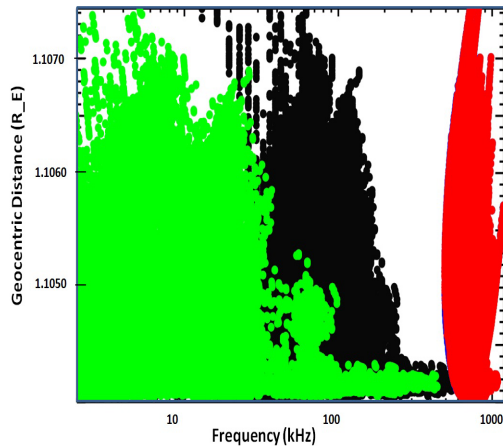


Figure 10. Variations of the frequency banded emission versus the geocentric distance expressed in R_E . The green, black and red colors are associated, respectively, to f_z , f_p and f_g frequencies.

We estimate the relationship between the Z-mode frequency (f_z), the plasma frequency (f_p) and the gyro-frequency (f_g) using the following formulae: $f_z = (f_g/2)[-1 + (1 + 4(f_p/f_g)^2)^{1/2}]$ (Carpenter et al., 2003). Fig.10 displays the variation of the three frequencies (i.e. f_z , f_p and f_g) versus the geocentric distance. The trapping region is localized between the lower and the higher f_z (green color in Fig.10) mainly between 1 kHz and 100 kHz, and extended up to 700 kHz. The plasma 5 frequency is following the trapping region and starting at about 10 kHz and up to 800 kHz. The gyro-frequency appears at higher frequencies, i.e. above 800 kHz. Those features are comparable to previous investigations, e.g. Gurnett et al. (1983) and Carpenter et al. (2003) in polar regions.

It is important to note that the frequency banded emissions may be due to the interaction and/or the co-existence of electrostatic and whistler waves. Hence Bell and Ngo (1990) considered theoretically the generation, in the case of density cavity 10 or gradient, of whistler waves by lower hybrid waves. Such co-existence of both waves have been investigated by An et al. (2017) using Darwin particle-in-cell (PIC) simulation. Such models have been recently invoked by Vartanyan et al. (2016) and Li et al. (2017) in the investigation, respectively, of generation of whistler waves and chorus wave modulation observed onboard DEMETER and Van Allen Probes satellites.

4 Conclusion

15 We have investigated the frequency banded wave radiation recorded by ICE/DEMETER experiment. DEMETER orbits allow us to regularly record this radiation where, in the optimal case, about 13 events are daily registered. The power level is found in the interval between $10^{-3} \mu Vm^{-1}Hz^{-1/2}$ and $10^{+4} \mu Vm^{-1}Hz^{-1/2}$. The spectral analysis leads to find a 'tree spectral shape' which is the traces of the beaming of the frequency banded wave radiation. We have shown that those beams are not similar and depend on the emission frequency and the magnetic latitude. DEMETER frequency banded emission can be 20 comparable to the well-known terrestrial kilometric radiation. However several other observational aspects are different when combining both emissions in particular the generation modes. We suggest that the DEMETER frequency banded emissions are linked to a Z-mode micro-scale region. This trapping Z-mode region can only be detected between the Earth's ionosphere and the plasmasphere. The hollow cones of this frequency banded wave emissions are crossed by the DEMETER orbits at altitudes lower than 700 km. Probably the source regions of the DEMETER frequency banded emission should be the plasmasphere, 25 like the terrestrial kilometric radiation. IMAGE investigations reported about density structures recorded by EUV experiment (Burch, 2000) where new terms have been defined like channels and crenulations (Darrouzet et al., 2009), and also a time evolution of the plasmasphere in particular on the pre-midnight sector (Sandel et al., 2003). We may consider that DEMETER orbits allow to investigate the inner part of the plasmasphere when other missions (i.e. GEOTAIL, IMAGE, INTERBALL) lead to study the outer part of the plasmasphere.

30 *Acknowledgements.* Acknowledgements. We acknowledge C. N. E. S. for the use of the DEMETER data, and thankful to Jean-Jacques Berthelier who provided us with data from the electric field experiment (Instrument Champ Électrique – ICE).

References

An, X., Bortnik, J., Van Compernolle, B., Decyk, V., and R. Thorne, Electrostatic and whistler instabilities excited by an electron beam, *Physics of Plasmas*, 24, 072116, 2017.

Bell, T.F., and H.D. Ngo, Electrostatic lower hybrid waves excited by electromagnetic whistler mode waves scattering from planar magnetic-field-aligned plasma density irregularities, *J. Geophys. Res.*, 95, A1, 149–172, 1990.

Berthelier, J.J., Godefroy, M., Leblanc, F., Malingre, M., Menvielle, M., Lagoutte, D., Brochot, J.Y., Colin, F., Elie, F., Legendre, C., Zamora, P., Benoist, D., Chapuis, Y., Artru, J., and R. Pfaff, ICE, the electric field experiment on DEMETER, *Planet. Space Sci.*, 54, 456–471, 2006.

Boudjada, M.Y., P.F. Biagi, E. Al-Haddad, P.H.M. Galopeau, B. Besser, D. Wolbang, G. Prattes, H. Eichelberger, G. Stangl, M. Parrot and K. Schwingenschuh, Reception conditions of low frequency (LF) transmitter signals onboard DEMETER micro-satellite, *Physics and Chemistry of the Earth*, 102, 70–79, 2017.

Brown, L.W., The galactic radio spectrum between 130 kHz and 2600 kHz, *Astrophys. J.*, 359–370, 1973.

Burch, J.L., IMAGE mission overview, *Space Sci. Rev.*, 91, 1–14, 2000.

Carpenter, D.L., Bell, T.F., Inan, U.S., Benson, R.F., Sonwalkar, V.S., Reinisch, B.W., and D. L. Gallagher, Z-mode sounding within propagation "cavities" and other inner magnetospheric regions by the RPI instrument on the IMAGE satellite, *J. Geophys. Res.*, 108, A12, 2003.

Darrouzet, F., Gallagher, D. L., André, N., Carpenter, D. L., Dandouras, I., Décréau, P. M. E., De Keyser, J., Denton, R. E., Foster, J. C., Goldstein, J., Moldwin, M. B., Reinisch, B. W., Sandel, B. R., and J. Tu, Plasmaspheric Density Structures and Dynamics: Properties Observed by the CLUSTER and IMAGE Missions, *Space Sci. Rev.*, 145, 55–106, 2009.

Décréau, P. M. E., Ducoin, C., Le Rouzic, G., Randriamboarison, O., Rauch, J.-L., Trotignon, J.-G., Vallières, X., Canu, P., Darrouzet, F., Gough, M. P., Buckley, A. M., and T.D. Carozzi, Observation of continuum radiations from the Cluster fleet: first results from direction finding, *Ann. Geophys.*, 22, 2607-2624, 2004.

Décréau, P. M. E., Fergeau, P., Krasnoselskikh, V., Le Guirriec, E., Lévéque, M., Martin, Ph., Randriamboarison, O., Rauch, J. L., Senée, F. X., Séran, H. C., Trotignon, J. G., Canu, P., Cornilleau, N., de Féraudy, H., Alleyne, H., Yearby, K., Mögensen, P. B., Gustafsson, G., André, M., Gurnett, D. C., Darrouzet, F., Lemaire, J., Harvey, C. C., Travnicek, P., and Whisper experimenters: Early results from the Whisper instrument on Cluster: an overview, *Ann. Geophys.*, 19, 1241-1258, 2001.

El-Lemdani Mazouz, F., J. L. Rauch, P. M. E. Décréau, J. G. Trotignon, X. Vallières, F. Darrouzet, P. Canu, and X. Suraud, Wave emissions at half electron gyroharmonics in the equatorial plasmasphere region: CLUSTER observations and statistics, *Adv. Space Res.*, 43, 253-264, 2009.

Goertz, C. K., and R. J. Strangeway, Plasma waves, in *Introduction to Space Physics*, edited by M. G. Kivelson and C. T. Russell, p. 356, Cambridge Univ. Press, New York, 1995.

Green, J. L., and S. A. Boardsen, Kilometric continuum radiation, *Radio Sci. Bull.*, 318, 34- 41, 2006.

Green, J. L., S. Boardsen, S. F. Fung, H. Matsumoto, K. Hashimoto, R. R. Anderson, B. R. Sandel, and B. W. Reinisch, Association of kilometric continuum radiation with plasmaspheric structures, *J. Geophys. Res.*, 109, A03203, 2004.

Grimald, S., and O. Santolik, Possible wave modes of wideband nonthermal continuum radiation in its source region, *J. Geophys. Res.*, 115, A06209, 2010.

Grimald, S., El-Lemdani Mazouz, F., Foullon, C., Décréau, P. M. E., Boardsen, S. A., and X. Vallières, X.: Study of non-thermal continuum patches: wave propagation and plasmapause study, *J. Geophys. Res.*, 116, A07219, 2011.

Grimald, S., Décréau, P. M. E., Canu, P., Rochel, A., and X. Vallières, Medium latitude sources of plasmaspheric non thermal continuum radiations observed close to harmonics of the electron gyrofrequency, *J. Geophys. Res.*, 113, A11217, 2008.

5 Gurnett, D. A., The Earth as a radio source: The nonthermal continuum, *J. Geophys. Res.*, 80, 2751–2763, 1975.

Gurnett, D. A., and L. A. Frank, Continuum radiation associated with low-energy electrons in the outer radiation zone, *J. Geophys. Res.*, 81, 3875–3885, 1976.

Gurnett, D. A., and R. A. Shaw, Electromagnetic radiation trapped in the magnetosphere above the plasma frequency, *J. Geophys. Res.*, 78, 8136- 8148, 1973.

10 Gurnett, D. A., Shawhan, S.D., and R. R. Shaw, Auroral hiss, Z-mode radiation, and auroral kilometric radiation in the polar magnetosphere: DE 1 observations, *J. Geophys. Res.*, 88, 329, 1983.

Hashimoto, K., J. L. Green, R. R. Anderson, and H. Matsumoto, Review of kilometric continuum, in *Geospace Electromagnetic Waves and Radiation*, Lect. Not. in Phys., Eds. J. W. LaBelle and R. A. Treumann, Springer, New York, 687, 37–54, 2006.

Hashimoto, K., W. Calvert, and H. Matsumoto, Kilometric continuum detected by GEOTAIL, *J. Geophys. Res.*, 104, 28,645- 28,656, 1999.

15 Jones, D., Source of terrestrial nonthermal radiation, *Nature*, 260, 686-689, 1976.

Kuril'chik, V.N., M. Y. Boudjada, H. O. Rucker, and I. F. Kopaeva, Observations of Electromagnetic Emissions inside the Earth's Plasmasphere from the INTERBALL-1 Satellite, *Cosmic Res.*, 45, 455–460, 2007.

Kuril'chik, V.N., Boudjada, M.Y. and H.O. Rucker, INTERBALL-1 observations of the plasmaspheric emissions related to terrestrial 'continuum' radio emissions, in *Planetary Radio Emissions V*, Eds. Rucker, H.O., Kaiser, M.L., and Leblanc, Y., Vienna: Austrian Academy of Sciences Press, 325–335, 2001.

20 Kurth, W. S., D. A. Gurnett, and R. R. Anderson, Escaping nonthermal continuum radiation, *J. Geophys. Res.*, 86, 5519–5531, 1981.

Li, J., Bortnik, J., An, X., Li, W., Thorne, R.M., Zhou, M., Kurth, W.S., Hospodarsky, G.B., Funsten, H.O., and H.E. Spence, Chorus Wave Modulation of Langmuir Waves in the Radiation Belts, *Geophys. Res. Lett.*, 44, 11713–11721, 2017.

Parrot M. and J.-J. Berthelier, AKR-like emissions observed at low altitude by the DEMETER satellite, *J. Geophys. Res.*, 117, A10314,

25 2012.

Parrot, M., U. S. Inan, N. G. Lehtinen, and J. L. Pincon, Penetration of lightning MF signals to the upper ionosphere over VLF ground-based transmitters, *J. Geophys. Res.*, 114, A12318, 2009.

Sandel, B.R., J. Goldstein, D.L. Gallagher and M. Spasojevic, Extreme ultraviolet imager observations of the structure and dynamics of the plasmasphere. *Space Sci. Rev.*, 109, 25-46 2003.

30 Sonwalkar, V.S., D.L. Carpenter, T.F. Bell, M. Spasojevic, U.S. Inan, J. Li, X. Chen, A. Venkatasubramanian, J. Harikumar, R.F. Benson, W.W.L. Taylor, and B. W. Reinisch, Diagnostics of magnetospheric electron density and irregularities at altitudes <5000 km using whistler and Z mode echoes from radio sounding on the IMAGE satellite, *J. Geophys. Res.*, 109, A11212, 2004.

Vartanyan, A., Milikh, G.M., Eliasson, B., Najmi, A.C., Parrot, M., and K. Papadopoulos, Generation of whistler waves by continuous HF heating of the upper ionosphere, *Radio Sci.*, 51, 1188–1198, 2016.